J Solid State Electrochem (2003) 7: 416–420
DOI 10.1007/s10008-002-0330-3

ORIGINAL PAPER

Rajendra N. Basu · Frank Tietz · Oliver Teller
Egbert Wessel · Hans Peter Buchkremer · Detlev Stöver

$LaNi_{0.6}Fe_{0.4}O_3$ as a cathode contact material for solid oxide fuel cells

Received: 29 May 2002 / Accepted: 11 September 2002 / Published online: 26 October 2002

Abstract In solid oxide fuel cells (SOFCs) the interconnects electrically link air and fuel electrodes on either side to produce a practical electrical power output. The long-term stability of intermediate temperature (650–800 °C) SOFC operation strongly depends on the composition of the ferritic steel interconnection material and the steel/ceramic interface. During high-temperature operation the Cr-containing ferritic steel forms an oxide scale at its surface, thereby causing high ohmic electrical contact resistance when connected to the surface of an electronically conducting ceramic cathode material. In the long run, the vaporization of Cr species from these oxide scales also affects the cathode activity, eventually leading to cell deterioration. One way of overcoming the problem is to incorporate another electronically conducting ceramic compliant layer, commonly known as the contact layer, between the cathode and metallic interconnect. In this contribution, $LaNi_{0.6}Fe_{0.4}O_3$ was tested as a cathode contact material. Its performance at 800 °C in the form of a ~50 μm thick film applied on two ferritic steel compositions was examined. After 600 h of testing, contact resistances of 60 and 160 $m\Omega\,cm^2$ were obtained. The different values are explained by the variation in steel composition.

Keywords Solid oxide fuel cell · Ferritic steel interconnect · Lanthanum nickel ferrite · Contact resistance

R.N. Basu · F. Tietz (✉) · O. Teller · E. Wessel
H.P. Buchkremer · D. Stöver
Forschungszentrum Jülich GmbH, Institute for Materials and Processing in Energy Systems (IWV), 52425 Julich, Germany
E-mail: f.tietz@fz-juelich.de
Tel.: +49-2461-615007
Fax: +49-2461-612455

Permanent address: R.N. Basu
Central Glass & Ceramic Research Institute, Calcutta 700 032, India

Present address: O. Teller
W.L. Gore & Associates GmbH, P.O. Box 1152, 85636 Munich, Germany

Introduction

Given that a single solid oxide fuel cell (SOFC) only produces less than one volt, individual cells are usually stacked together, anode-to-cathode, to produce a more substantial voltage as electrical output from the SOFC device during operation at high temperature. Thus an interconnect material is used to connect the anode of one cell to the cathode of another. The interconnect must be electrically conducting, gastight and have a matching thermal expansion coefficient (TEC) to that of the other cell components [1, 2]. Both ceramic (doped $LaCrO_3$) and metal interconnects are used by SOFC developers, depending on the particular cell design and stacking concept. However, for intermediate-temperature (650–800 °C) operation, low-cost ferritic steel interconnects are now being widely used [3, 4, 5], though problems due to poor electrical contacts between metallic interconnects and electrodes are reported in the literature [6, 7]. Normally, these steels are high Cr-containing steels (>20 wt%). The presence of Cr in the ferritic steel composition forms a very thin, electronically poorly conductive chromia scale on the surface of the interconnect, which in principle should prevent further oxidation of the metal interconnect while the fuel cell is operating at high temperature (>650 °C) in an oxidizing atmosphere. In addition to the increase in ohmic contact resistance, the vaporization of chromium oxyhydroxides [8] from these oxide scales during operation also affects the catalytic activity of the cathode and causes cell degradation. One of the ways of overcoming such a problem is to incorporate compliant layers on both the anode and cathode side [2]. As these coatings protect the interconnects, they are also termed contact or protective layers. The contact materials must have high electrical conductivity, matching thermal expansions, and chemical stability, particularly with respect to the electrodes to be connected and the interconnect. Normally, on the fuel side (anode), the contact is made of a nickel mesh that is

welded to the metallic interconnect. On the oxidant side (cathode), a thick film is deposited which is normally a perovskite (e.g. $LaCoO_3$ [9]). Recently, a variety of such cathode contact layers have been reported in the literature [10, 11, 12, 13, 14, 15].

In this paper, $LaNi_{0.6}Fe_{0.4}O_3$ (LNF) [16] was tested as a cathode contact material. According to Chiba et al. [16], the series $LaNi_{1-x}Fe_xO_3$ has an orthorhombic or hexagonal perovskite structure at room temperature when $x > 0.5$ or $x = 0.4$, respectively. For $x < 0.4$, two-phase mixtures were observed [16]. The performance of LNF thick films applied on two ferritic steel compositions was evaluated at 800 °C.

Experimental

In the present investigation, two model ferritic steel compositions, FeCr(Mn) and FeCr(Mn,La,Ti) [10], were used. The only difference between the two is the addition of small amounts of reactive elements (La and Ti). The LNF powder was prepared by the citrate-nitrate gel technique [17]. In this technique, a gel is formed from the mixed metal nitrate solutions in the presence of citrate. The mixture of nitrates and citrate was then finally ignited as a result of the thermally induced oxidation-reduction reaction. Upon calcination at 700 °C for 3 h in air, the ash obtained from the ignition yields the desired powder. Further grinding in a planetary mill under ethanol for about a day produces ultra-fine powder having a mean particle size of $d_{50} \approx 0.3$ μm. A screen-printing paste was prepared using this ultra-fine powder together with ethyl cellulose and terpineol as binder and solvent, respectively. This paste was then applied by screen printing on the polished and cleaned surfaces of the above-mentioned two steel compositions. The thickness of the particulate films was about 50 μm. The samples were placed inside a furnace and maintained at 800 °C in air. At this temperature, sintering of the powder particles is very limited, although the preparation route yields fine powders. Therefore the porosity of the ceramic coating is typically in the range of 40–55% and the effective contact area is approximately half of the geometrical size of the samples.

The procedure for electrical and microstructural characterizations was the same as described elsewhere [10]. The reproducibility of the set-up for the contact resistance measurements was tested prior to the work with other ceramic materials and an experimental error of 10–15% was found.

Crystalline phase analysis was carried out using a Siemens D5000 diffractometer using Cu K_α radiation. Thermal expansion measurements on the materials listed in Tables 1 and 2 were carried out with a Netzsch DIL 402C dilatometer. The ceramic and metallic samples were measured in air and in dried argon flowing through two powder columns of Sicapent (Merck), respectively. Sample preparation and further experimental details were previously reported elsewhere [18, 19].

Table 1 Comparison of electrical conductivities of LNF, LSM and $LaCoO_3$ at 700, 800 and 900 °C

Material	σ at 700 °C ($S\ cm^{-1}$)	σ at 800 °C ($S\ cm^{-1}$)	σ at 900 °C ($S\ cm^{-1}$)
$LaNi_{0.6}Fe_{0.4}O_3$ (LNF)	313	305	297
$La_{0.65}Sr_{0.3}MnO_3$ (LSM)	233	228	228
$LaCoO_3$ [18]	–	700	–

Table 2 TEC values of LNF, LSM, $LaCoO_3$, FeCr(Mn) and FeCr(Mn,La,Ti) between room temperature and different measurement temperatures

	Thermal expansion coefficient (K^{-1})×10^{-6}		
	700 °C	800 °C	900 °C
$LaNi_{0.6}Fe_{0.4}O_3$ (LNF)	11.5	11.8	12.1
$La_{0.81}Sr_{0.19}MnO_3$ (LSM) [19]	–	10.8	–
$La_{0.7}Sr_{0.3}MnO_3$ (LSM) [19]	–	11.7	–
$La_{0.65}Sr_{0.3}MnO_3$ (LSM)	12.4	12.5	12.6
$LaCoO_3$	22.9	22.5	22.2
FeCr(Mn)	11.7	12.2	12.7
FeCr(Mn,La,Ti)	11.6	11.9	12.2

Results and discussion

The XRD pattern of the as-calcined LNF powder is shown in Fig. 1 (bottom). The large peaks correspond to a rather disordered perovskite, whereas the other broader reflections tentatively can be related to NiO and La_2NiO_4-type structures. Already after heat treatment at 800 °C only perovskite reflections are visible. However, the material consists of a mixture of mainly a hexagonal perovskite and minor amounts of an orthorhombic perovskite (only visible in Fig. 1 as shoulders on the left-hand side of the hexagonal reflections). Sintering at 900 °C yields a single-phase hexagonal LNF powder [16]. The lattice parameters measured on powder sintered at 1400 °C (the pattern is the same as the one measured after sintering at 900 °C as shown in Fig. 1) gave $a = 5.504(2)$ Å and $c = 13.246(5)$ Å.

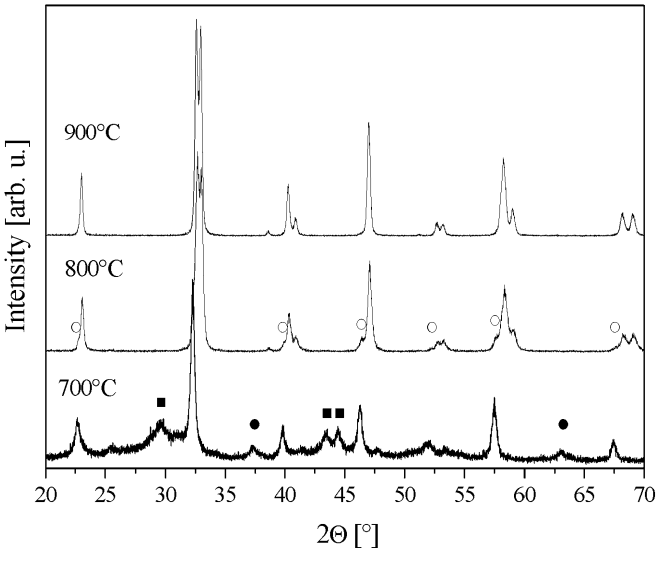

Fig. 1 XRD patterns of LNF after heat treatments at 700 °C for 3 h, 800 °C and 900 °C for 5 h (*from bottom to top*). The *filled circles* and *squares* tentatively correspond to reflections of NiO and La_2NiO_4, respectively; the *open circles* correspond to reflections of an orthorhombic perovskite

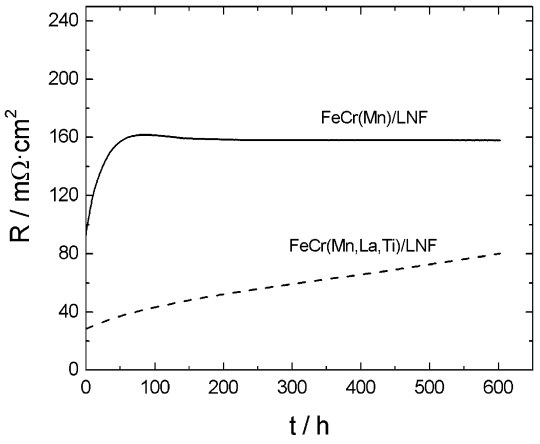

Fig. 2 Electrical resistance of the material combinations FeCr(Mn)/LNF (*solid line*) and FeCr(Mn,La,Ti)/LNF (*dashed line*). Experimental conditions: $T = 800$ °C, $p(O_2) = 0.21$ bar and $j = 150$ mA cm^{-2}

Figure 2 shows the electrical resistances of the material combinations FeCr(Mn)/LNF and FeCr(Mn,La,-Ti)/LNF as a function of time. The FeCr(Mn,La,Ti)/LNF combination shows a low contact resistance, which increases steadily with time during the investigated exposure time. In contrast, the FeCr(Mn)/LNF combination starts at a higher resistance value but remains constant after about 70 h at a level of 150 mΩ cm^2. The results after 600 h of continuous running reveal almost negligible variations in contact resistance (Fig. 2). Remarkably, the electrical conductivity and thermal expansion coefficient (TEC) values of $LaNi_{0.6}Fe_{0.4}O_3$ are very favorable compared to the two most commonly used cathode contact materials of $La_{1-x-y}Sr_xMnO_3$ (LSM) and $LaCoO_3$. Although $LaCoO_3$ offers an excellent conductivity value (700 S cm^{-1} at 800 °C) [20], it allows only limited thermal cycling because of its extremely high TEC value ($> 20\times10^{-6}$ K^{-1}) (Tables 1 and 2). On the other hand, LNF shows a perfectly matching TEC with that of other cell components, including the two steel compositions (Table 2), comparable with stoichiometric LSM [21]. In addition, it offers a moderate conductivity value (~300 S cm^{-1} at 800 °C), which is significantly higher than that of LSM (Table 1). Therefore, it is expected that when LNF is used as a cathode contact layer its contact resistance change (with steel) is primarily due to differences in the steel compositions. For further clarification an extensive microstructural investigation was performed on both FeCr(Mn)/LNF and FeCr(Mn,La,Ti)/LNF after termination of 600 h of continuous exposure at 800 °C.

Figure 3 shows the polished cross-sections of two interfaces between FeCr(Mn)/LNF (left) and FeCr(Mn,La,Ti)/LNF (right). In both cases a Cr_2O_3 layer with significant amounts of Mn was formed. The amount of Mn detected by EDX analysis is as shown in Fig. 4. As the manganese is a minor component in the steel composition, the interface layer is therefore better described as a $Cr_2O_3/(Cr,Mn)_3O_4$ corrosion scale [5, 10]. In addition, the FeCr(Mn,La,Ti) steel shows internal oxidation due to the Ti and La doping. Since in both cases the corrosion layer seems to be very similar, it is very difficult to predict the reason for the different results in electrical resistance measurements. However, the higher resistance and stable performance of FeCr(Mn)/LNF might be caused by the absence of Ti and La in this steel composition, leading to a more stable and crystallographically more perfect corrosion scale, which therefore shows higher resistance and effective protection against further corrosion. This result is also in good agreement with the thickness of the interface layers formed. A closer look indicates that in the case of FeCr(Mn) the corrosion scale is slightly thinner than that of FeCr(Mn,La,Ti) (Fig. 3). Both the elements (La and Ti) formed their oxides during the experiment (long-time exposure at 800 °C in air) and are also incorporated in the corrosion scales as dopants, leading to defects in the crystal lattice and therefore to lower resistances. However, these defects increase the material transport across the interface layers and may explain the minor protection against corrosion causing the small and steady increase in resistance due to ongoing scale growth.

For better understanding of the occurring chemical processes, an FeCr(Mn,La,Ti)/LNF sample was exposed for 500 h at 800 °C and examined by XRD. After the annealing time the contact layer was carefully scraped off from the metal substrate and both the powder

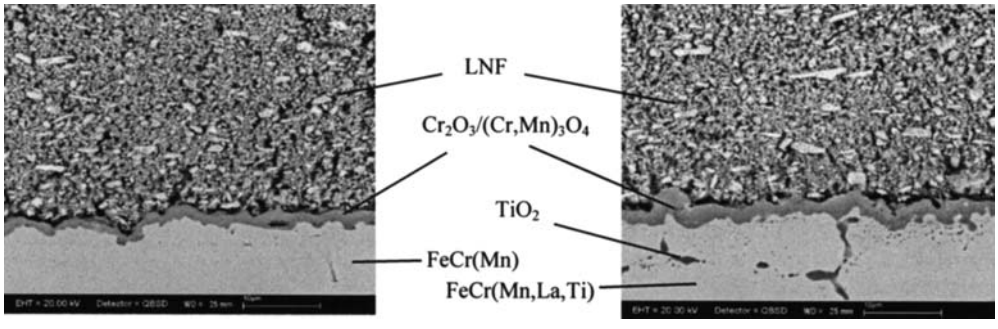

Fig. 3 SEM images of the material combinations FeCr(Mn)/LNF (*left*) and FeCr(Mn,La,Ti)/LNF (*right*) after exposure. Experimental conditions: $T = 800$ °C, $p(O_2) = 0.21$ bar, $t = 600$ h and $j = 150$ mA cm^{-2}

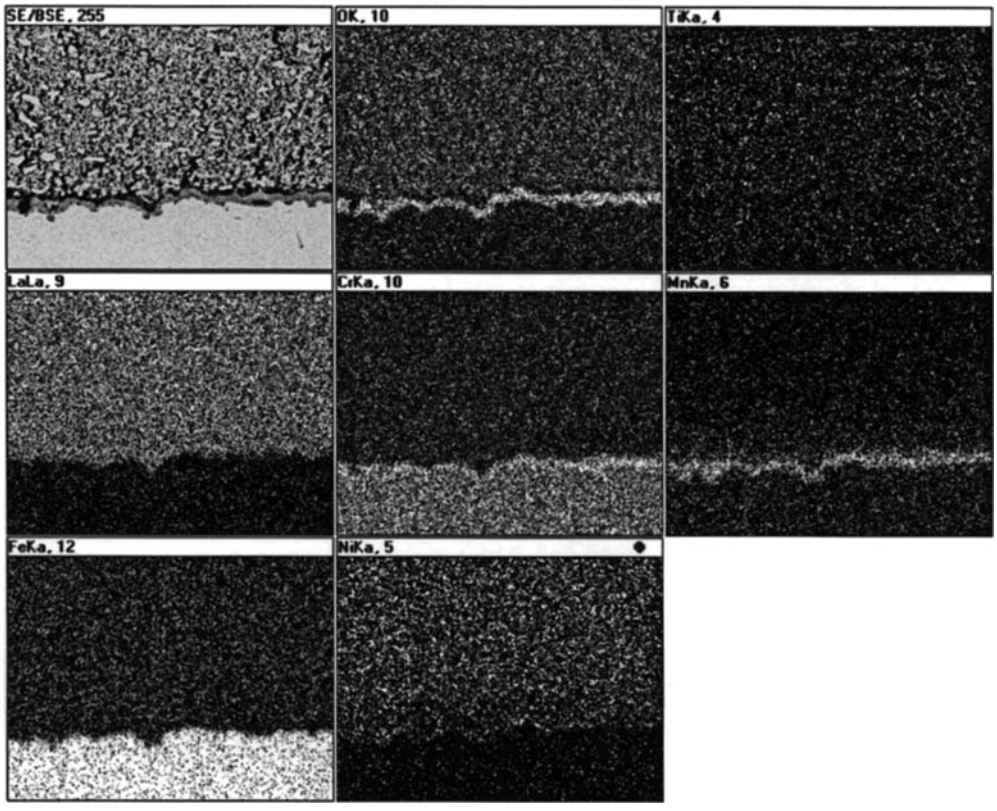

Fig. 4 SEM image (*top left*) and element mapping of the material combination FeCr(Mn)/LNF. Experimental conditions: $T = 800$ °C, $p(O_2) = 0.21$ bar, $t = 600$ h and $j = 150$ mA cm^{-2}

obtained and the remaining substance on the substrate were separately analyzed. The obtained XRD patterns are shown in Fig. 5 together with the initial powder pattern of LNF (pattern a). Three significant changes in the perovskite pattern (b) were observed: (1) the initial hexagonal LNF transformed to an orthorhombic perovskite; (2) the perovskite reflections shifted towards smaller 2Θ values, i.e. the dimension of the unit cell increased; (3) NiO was formed during the exposure. Some small additional spinel peaks were observed, but these reflections are much more intense in pattern (c) of Fig. 5, i.e. the oxide scale composed of chromia and spinel was strongly bonded on the metal substrate.

Furthermore, two aspects are interesting to note. Firstly, the Ni distribution in the contact layer in both material combinations is depleted towards the steel interface. The consequences or the influence of Ni on the resistance has not yet been explored in detail, but it seems that the contact layer undergoes a chemical reaction. Because chromium species are released from the steel and the $Cr_2O_3/(Cr,Mn)_3O_4$ corrosion scale does not act as a perfect barrier for these chromium species [8], it is assumed that the perovskite is partially substituted by chromium. This would explain, on the one hand, the crystallographic changes of the material and, on the other hand, the release of NiO. However, this reaction scheme cannot be visualized within the resolution limit

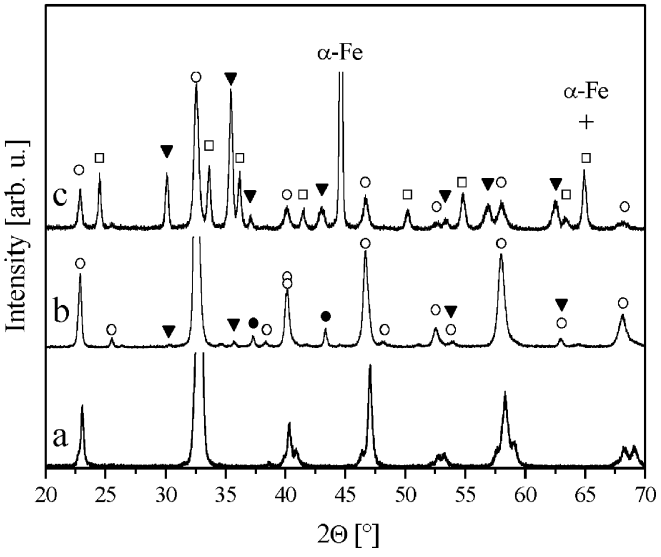

Fig. 5 XRD patterns of (*a*) the initial LNF powder after calcination at 800 °C (cf. Fig. 1); (*b*) the LNF powder after annealing at 800 °C for 500 h on top of an FeCr(Mn,La,Ti) substrate (*open circles* belong to orthorhombic perovskite structure, *filled circles* to NiO and *filled triangles* to spinel structure); (*c*) the remaining substance on the FeCr(Mn,La,Ti) substrate (*open circles* and *filled triangles* as before; *open squares* belong to Cr_2O_3)

of the element mappings in Fig. 4. Secondly, no layer of alkaline-earth chromates is formed, as reported by several authors [10, 12, 13, 15], owing to the avoidance of such elements in the perovskite. Therefore the interface seems to be thinner, denser and less vulnerable to

thermal cycles in comparison with the severe interfacial reactions observed by Malkow et al. [22, 23], who exposed a commercial ferritic steel (X 10 CrAl 18) with Sr-containing LNF at 800 °C for 300 h. They observed a 30 μm thick reaction zone instead of 1–2 μm for FeCr(Mn)/LNF and 2–3 μm for FeCr(Mn,La,Ti)/LNF (see Fig. 2 left and right, respectively). The reasons for the very different corrosion behavior are, on the one hand, the Mn content in the model steels forming a $Cr_2O_3/(Cr,Mn)_3O_4$ corrosion scale (Fig. 4) which protects the perovskite from enhanced chromia contamination [3, 5] and, on the other hand, the absence of alkaline-earth elements in the perovskite preventing chromate formation (as also happened in the case of X 10 CrAl 18 [22, 23]) as mentioned above, thus thermodynamically and chemically stabilizing the perovskite [24, 25].

Conclusions

The use of $LaNi_{0.6}Fe_{0.4}O_3$ as a cathode contact layer for SOFC shows promising performances while operating in the cathodic configuration using two ferritic steel interconnects for about 600 h at 800 °C in an oxidizing atmosphere. Particularly, the presence of La and Ti in the steel compositions might be effective when LNF is used as a protective coating. However, further long-time exposures (more than the 600 h in the experiment) are necessary to observe the contact resistance behavior in depth. Probably minor compositional changes in the steel interconnect may give even better results in order to achieve the optimum material combination between the ceramic and the steel. The avoidance of alkaline-earth elements in the contact material seems to be the right way to proceed.

Acknowledgement The authors are grateful to Mr. A. Gupta, Mr. W. Jungen and Mr. P. Lersch for their technical support. Financial support from the German Federal Ministry of Economics and Technology under contract no. O327088C/8-1A is gratefully acknowledged.

References

1. Minh NQ, Takahashi H (1995) Science and technology of ceramic fuel cells. Elsevier, New York
2. Badwal SPS, Foger K (1997) Mater Forum 21:187
3. Quadakkers WJ, Malkow T, Pirón-Abellán J, Flesch U, Shemet V, Singheiser L (2000) In: McEvoy AJ (ed) Proceedings of the European SOFC forum IV, vol. 2. Oberrohrdorf, Switzerland, pp 827–836
4. Honegger K, Plas A, Diethelm R, Glatz W (2001) In: Yokokawa H, Singhal SC (eds) Proceedings of the 7th international symposium on SOFC (SOFC-VII). (Electrochemical Society proceedings series, PV 2001-16) Electrochemical Society, Pennington, NJ, pp 803–810
5. Pirón-Abellán J, Shemet V, Tietz F, Singheiser L, Quadakkers WJ (2001) In: Yokokawa H, Singhal SC (eds) Proceedings of the 7th international symposium on SOFC (SOFC-VII). (Electrochemical Society proceedings series, PV 2001-16) Electrochemical Society, Pennington, NJ, pp 811–819
6. de Haart LGJ, Mayer K, Stimming U, Vinke IC (1998) J Power Sources 71:302
7. Hou PY, Huang K, Bakker WT (1999) In: Singhal SC, Dokiya M (eds) Proceedings of the 6th international symposium on SOFC (SOFC-VI). (Electrochemical Society proceedings series, PV 99-19) Electrochemical Society, Pennington, NJ, pp 737–748
8. Gindorf Ch, Singheiser L, Hilpert K (2001) Steel Res 72:528
9. Buchkremer HP, Diekmann U, de Haart LGJ, Kabs H, Stimming U, Stöver D (1997) In: Stimming U, Singhal SC, Tagawa H, Lehnert W (eds) Proceedings of the 5th international symposium on solid oxide fuel cells (SOFC-V). (Electrochemical Society proceedings series, PV 97-18) Electrochemical Society, Pennington, NJ, pp 160–170
10. Teller O, Meulenberg WA, Tietz F, Wessel E, Quadakkers WJ (2001) In: Yokokawa H, Singhal SC (eds) Proceedings of the 7th international symposium on SOFC (SOFC-VII). (Electrochemical Society proceedings series, PV 2001-16) Electrochemical Society, Pennington, NJ, pp 895–903
11. Yoo Y, Dauga M (2001) In: Yokokawa H, Singhal SC (eds) Proceedings of the 7th international symposium on SOFC (SOFC-VII). (Electrochemical Society proceedings series, PV 2001-16) Electrochemical Society, Pennington, NJ, pp 837–846
12. Larring Y, Norby T (2000) J Electrochem Soc 147:3251
13. Quadakkers WJ, Greiner H, Hänsel M, Pattanaik A, Khanna AS, Malléner W (1996) Solid State Ionics 91:55
14. Ruckdäschel R, Henne R, Schiller G, Greiner H (1997) In: Stimming U, Singhal SC, Tagawa H, Lehnert W (eds) Proceedings of the 5th international symposium on solid oxide fuel cells (SOFC-V). (Electrochemical Society proceedings series, PV 97-18) Electrochemical Society, Pennington, NJ, pp 1273–1282
15. Shiomitsu T, Kadowaki T, Ogawa T, Maruyama T (1995) In: Dokiya M, Yamamoto O, Tagawa H, Singhal SC (eds) Proceedings of the 4th international symposium on solid oxide fuel cells (SOFC-IV). (Electrochemical Society proceedings series, PV 95-1) Electrochemical Society, Pennington, NJ, pp 850–857
16. Chiba R, Yoshimura F, Sakurai Y (1999) In: Singhal SC, Dokiya M (eds) Proceedings of the 6th international symposium on SOFC (SOFC-VI). (Electrochemical Society proceedings series, PV 99-19) Electrochemical Society, Pennington, NJ, pp 453–462
17. Tietz F, Arul Raj I, Jungen W, Stöver D (2001) Acta Mater 49:803
18. Tietz, F (1999) In: Vincenzini P (ed) Proceedings of the 9th CIMTEC world ceramic congress and forum on new materials, vol 24 (Innovative materials in advanced energy technologies). Techna, Faenza, Italy, pp 61–70
19. Tietz F (1999) Ionics 5:129
20. Mineshige A, Inaba M, Yao T, Ogumi Z, Kikuchi K, Kawase M (1996) J Solid State Chem 121:423
21. Hammouche A, Siebert E, Hammou A (1989) Mater Res Bull 24:367
22. Malkow Th (1998) PhD thesis, RWTH Aachen
23. Malkow Th, Quadakkers WJ, Singheiser L, Nickel H (1998) Ber Forschungszentrums Jülich, Jül-3589. Forschungszentrum Jülich, Germany
24. Tanasescu S, Totir ND, Marchidan DI (1998) Electrochim Acta 43:1675
25. Ullmann H, Trofimenko N, Tietz F, Stöver D, Ahmad-Khanlou A (2000) Solid State Ionics 138:79